Hysteresis of the martensitic phase transition in magnetocaloric-effect Ni-Mn-Sn alloys

P. J. Shamberger and F. S. Ohuchi
Department of Materials Science and Engineering, University of Washington, Seattle, Washington 98195, USA
(Received 10 October 2008; revised manuscript received 2 February 2009; published 8 April 2009)

We have investigated the hysteresis of the temperature- and magnetic field–induced martensitic phase transition in $Ni_{50.4}Mn_{34.0}Sn_{15.6}$. Specifically, we have characterized the fraction of martensite and cubic Heusler phase present along a variety of temperature and magnetic field paths using magnetization as a proxy for the fraction of phases present. We present these results and discuss (1) the thermodynamics of the thermal- and magnetic field–induced hysteresis and (2) the impact of this hysteresis on the magnetocaloric effect of the alloy. We demonstrate that both temperature and magnetic field are equivalent driving forces for the phase transition and result in equivalent hysteresis behavior linked through the magnetic Gibbs free energy. The hysteresis reduces the useful magnetocaloric effect of the alloy by allowing only a limited fraction of the alloy to transform cyclicly between the martensite and the austenite phase under application and removal of magnetic fields up to 9 T, and by dissipating work through irreversible energy loss. While the importance of a large thermodynamically reversible magnetic entropy change is generally accepted, our results suggest that the hysteresis behavior is equally critical in evaluating the effective magnetocaloric effect of a material.

DOI: 10.1103/PhysRevB.79.144407 PACS number(s): 81.30.Kf, 75.30.Sg, 64.70.kd, 65.40.gd

I. INTRODUCTION

The magnetocaloric effect (MCE) describes the temperature and entropy changes in a material that result from a change in applied magnetic field. The temperature and entropy components of the MCE are defined as the adiabatic temperature change (ΔT_{ad}) and the isothermal magnetic entropy change (ΔS_M). In MCE materials, an applied field induces an alignment of magnetic moments, thereby altering the spin (magnetic) entropy of the system.[1,2] Spin-lattice coupling links changes in spin entropy to changes in lattice entropy, resulting in the observed temperature change. MCE materials are very promising as magnetic refrigerants in next-generation refrigeration technology due to their high efficiency and ability to replace environmentally harmful vapor refrigerants.[3,4] To function in this capacity, MCE materials require a large ΔS_M over a wide range in temperature, indicating that they can accomplish substantial thermodynamically reversible work over each refrigeration cycle.[5] Multiple factors may subtract from the reversible work achievable by a given material, including kinetic limitations, irreversible phase transitions, and hysteretic losses.[6–11]

First-order phase transitions may lead to very large ΔS_M, as first demonstrated in the "giant" MCE material $Gd_5(Ge,Si)_4$.[12,13] Since this finding, a number of other material systems with first-order phase changes have been investigated, including MnFe(P,As),[14] Mn(As,Sb),[15] $La(Fe,M)_{13}$,[16] and Ni-Mn-X (X=Ga,In,Sn,...) Heusler alloys.[17,18] In these systems, the ΔS_M is caused primarily by the entropy difference between the two phases, while the ΔT_{ad} is attributed to the change in the transition temperature caused by the applied field.[19] This ΔS_M tends to be very large, attracting a high degree of interest in these materials. However, in many cases, the quantity of useful work achievable in a single refrigeration cycle is largely diminished by hysteresis losses around the first-order phase transition.[10,20]

The Ni-Mn-X (X=Sn,In) Heusler alloy system is a particularly interesting class of materials due to the large reported inverse MCE.[18,20] In these materials, an increase in applied field causes a decrease in the temperature of the material, the opposite response to what is typically observed. The MCE in the Ni-Mn-X (X=Sn,In) system is the result of a martensitic phase change that is controlled by temperature, stress, or an external magnetic field.[21,22] Martensitic phase changes are diffusionless transitions that are typically very rapid (e.g., Ref. 23). In the Ni-Mn-X family, this transition is known to be highly reproducible, but to be accompanied by a thermal hysteresis, typically ~10–50 K.[21,24]

Further advancement of first-order phase change materials toward the ultimate goal of practical magnetic refrigeration requires an improved understanding of their hysteretic behavior around the phase transition. Specifically, it is not well understood how the hysteresis of most first-order phase change materials behaves under the complex temperature and magnetic field path that a working magnetic refrigerant is likely to follow, nor is it well characterized how the hysteresis of most materials affects their potential use as magnetic refrigerants. Of particular interest in this study is the measurement of energy loss due to hysteresis as this quantity directly decreases the efficiency of a magnetic refrigeration cycle and is rarely reported in studies of MCE materials. To these ends, we report here the temperature- and field-dependent martensitic transformation of a representative polycrystalline Heusler alloy, $Ni_{50.4}Mn_{34}Sn_{15.6}$.

II. EXPERIMENT

A bulk Ni-Mn-Sn alloy sample was prepared by melting ~4 g of >99.95% purity starting metals under a positive pressure of Ar in an arc-melting furnace. The furnace was purged three times and a Ti getterer was melted prior to melting the sample in order to remove oxygen from the system. The Ni-Mn-Sn alloy was melted and turned three times to homogenize it. The sample was weighed before and after melting and lost less than 1 wt % mass. This loss was attributed to Mn volatility, as a thin layer of Mn powder formed

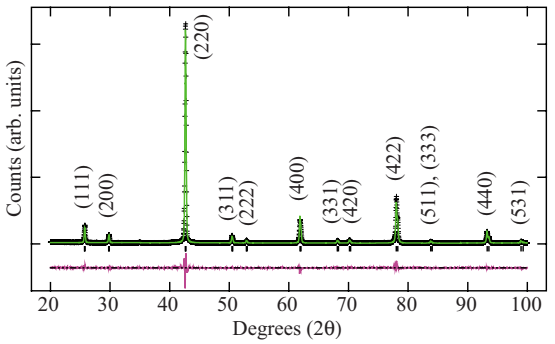

FIG. 1. (Color online) Room temperature x-ray diffraction scan of $Ni_{50.4}Mn_{34.0}Sn_{15.6}$ alloy, collected with Cu $K\alpha$ radiation. Pattern is indexed and fit assuming a cubic $L2_1$ structure with excess Mn occupying vacant Sn sites (a=0.59936 nm, χ^2=5.665).

around the well during melting. After melting, the alloy was annealed at 1200 K for 24 h in a quartz tube, open on one end, under a continuous vacuum of less than 2×10^{-6} torr. It was cooled slowly (~10 K/min) in the furnace to promote atomic ordering.

Chips from the interior portion of the sample (untouched by blades or polishing grit) were set aside for magnetic characterization and compositional analysis. The final alloy composition was determined by wavelength dispersive spectrometry (WDS) using a JEOL 733 electron microprobe. The composition of the alloy, determined as the average of multiple points on two separate alloy chips and given in atomic percent (2σ), is Ni=50.4(0.2), Mn=34.0(0.3), and Sn =15.6(0.2). The reported composition is an average of multiple points on two separate alloy chips; no compositional heterogeneity was observed on the micrometer and millimeter length scales. The alloy composition is within 1 at % of the premelting composition. Powder x-ray diffraction (XRD) was performed at room temperatures in order to verify which phases were present. XRD scans were collected with a Siemens D5000 $\theta-2\theta$ x-ray diffractometer using Cu $K\alpha$ radiation. The 2θ angular scale was calibrated with the NIST1976 corundum XRD standard and its estimated absolute uncertainty is $\pm0.035°2\theta$. Resulting XRD scans were analyzed with the Rietveld fitting software GSAS.[25] Only the Heusler phase ($L2_1$ structure) is present (Fig. 1). Peak intensities agree with Ni occupying the ($8c$) lattice sites, Sn occupying ($4a$) sites, and Mn occupying both ($4b$) and the remaining ($4a$) sites.

Magnetic characterization was performed with a vibrating sample magnetometer (VSM) in a Quantum Design physical properties measurement system (PPMS) on a small (~5 mg) equant alloy chip. Heating and cooling rates were limited to 1 °C/min. Faster rates of change (e.g., 5 °C/min) led to significantly wider hysteresis loops [see Fig. 2(b), inset], while slower rates (e.g., 0.5 °C/min) produced no significant decrease in the hysteresis width. The rate of 1 °C/min was chosen to reduce instrumental lag caused by thermal heterogeneity in the sample, while still allowing for the practical conduction of the experiment. The kinetics of structural and magnetic relaxations in these samples are the subject of ongoing investigation. Magnetic field was changed at a rate of 0.002 T/s.

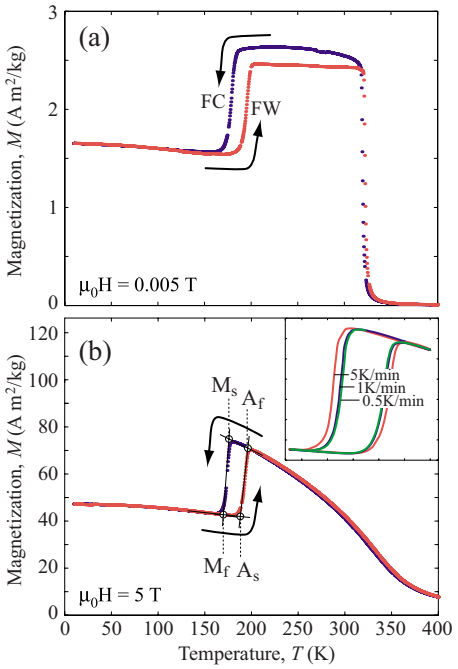

FIG. 2. (Color online) Field cooling (blue/dark gray data points) and field warming (red/light gray data points) magnetization curves for $Ni_{50.4}Mn_{34.0}Sn_{15.6}$ Heusler alloy at (a) low (0.005 T) and (b) moderate (5 T) magnetic fields. Arrows illustrate direction of temperature change. Transformation temperatures (martensite start, M_s, martensite finish, M_f, austenite start, A_s, austenite finish, A_f) are defined as the intersection of the extrapolation from the linear regions. Inset in (b) shows effect of heating and cooling at different rates.

III. RESULTS

A. Thermal hysteresis

Magnetization of the alloy was measured at a constant applied field (Fig. 2) first while decreasing the temperature from above the Curie temperature (field cooling, "FC"), and second while increasing the temperature (field warming, "FW"). A distinct step in magnetization is observed at ~170–190 K, due to the lower magnetization of the martensite phase relative to the cubic $L2_1$, parent Heusler phase (henceforth referred to as "austenite").[21] An overheating and an undercooling are required to transform martensite to austenite and austenite to martensite, respectively, resulting in a thermal hysteresis loop. Characteristic temperatures of the transformation (martensite start, M_s, martensite finish, M_f, austenite start, A_s, and austenite finish, A_f) are defined as the intersections of extrapolations from linear regions of data, as illustrated in Fig. 2(b). At low fields, magnetization is history dependent at temperatures significantly above A_f [Fig. 2(a)] and below M_f (not shown), suggesting the presence of coexisting antiferromagnetic (AFM) coupling in the system that is modified during the martensitic transformation.

Repeated thermal cycles through different extents of transformation define partial thermal hysteresis loops, allowing us to investigate the temperature dependence of the forward and reverse transformation (Fig. 3). Heating cycles were initiated well below the phase transition (160 K), and

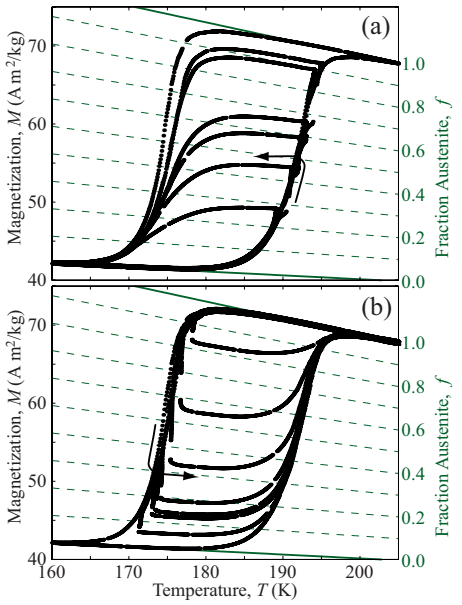

FIG. 3. (Color online) Partial thermal hysteresis loops obtained by (a) heating cycles and (b) cooling cycles under an applied field of $\mu_0 H = 5$ T. Arrows illustrate direction of temperature change. Green/gray dashed lines indicate the fraction of austenite present, following the methods described in the text.

warm the sample through various degrees of completion of the phase transformation, before cooling the sample back to the initial temperature. Cooling cycles proceed in the opposite sense and were initiated well above the phase transition (205 K). Thermal cycles at low field (0.005 T, not shown) are qualitatively similar to those illustrated in Fig. 3.

Magnetization data were transformed to $f(T)$, the mass fraction of austenite present, by assuming that total magnetization is proportional to the mass fraction of austenite and martensite phases (Fig. 4). Magnetization of pure martensite and austenite phases for a given temperature were determined by linearly extrapolating FC and FW curves across the phase transition. This allows for a linear mapping from magnetization, $M(T)$, to fraction of austenite, $f(T)$, as illustrated by the dashed lines in Fig. 3. FC and FW curves, which extend to temperatures well below and well above the transition, form an envelope that defines the maximum fraction of austenite and martensite possible for a given temperature, respectively (Fig. 4). Forward transformations in both heating and cooling cycles follow this outer envelope defined by FC and FW curves. Very little reverse transformation occurs in the heating (and cooling) cycles until the temperature has cooled below (heated above) the mean midpoint between FC and FW curves.

B. Magnetic hysteresis

Magnetization of the alloy was measured at a constant temperature while applying and removing an external magnetic field (magnetic hysteresis curves). Magnetic hysteresis curves were first measured at temperatures above (210 K) and below (160 K) the transition to record the intrinsic magnetic properties of the austenite and martensite phases, respectively (Fig. 5). Both phases are magnetically soft, expressing negligible magnetic hysteresis, and approaching saturation at low applied field (~0.3 T for the austenite phase and ~0.5 T for the martensite phase). However, due to the presence of antiferromagnetic interactions in both phases, a portion of the atomic moments is aligned antiparallel to the direction of spontaneous magnetization. Rotation of these moments in large magnetic fields determines the linear dependence of magnetization above saturation. The martensite phase has a significantly lower magnetization than the cubic Heusler phase over all magnetic fields up to 9 T (Fig. 5).

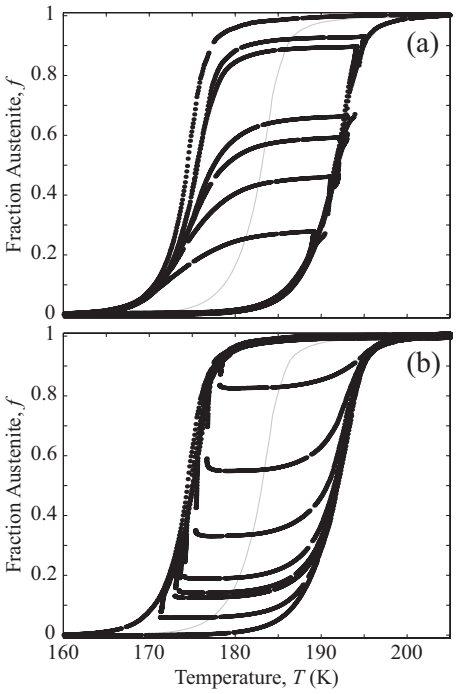

FIG. 4. Temperature vs mass fraction of austenite, calculated from data in Fig. 3 for (a) heating cycles and (b) cooling cycles, as described in the text. Gray midline represents mean transformation temperature.

Magnetic hysteresis curves were also measured at 190 K following two distinct approaches: (i) The sample was first

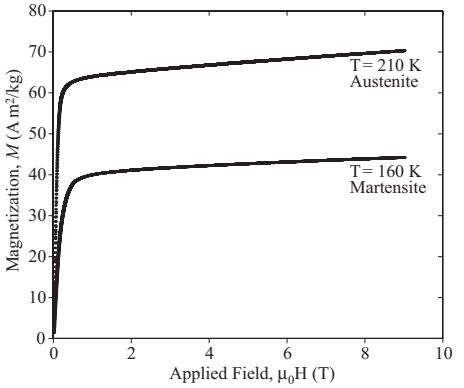

FIG. 5. Magnetic hysteresis loops of pure martensite (160 K) and pure austenite phase (210 K).

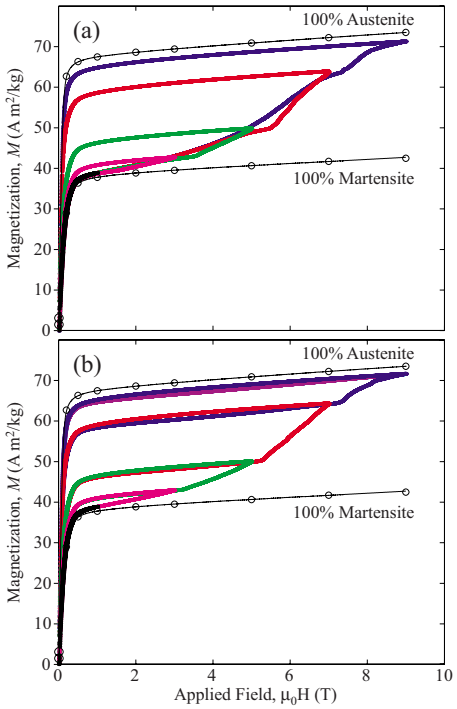

FIG. 6. (Color online) Magnetic hysteresis loops taken at $T = 190$ K following (a) method i—sample is cooled between each magnetic hysteresis loop—and (b) method ii—sample remains at 190 K throughout the measurement. Approximated pure martensite and austenite phase hysteresis curves (circles and thin black line) are determined as described in the text.

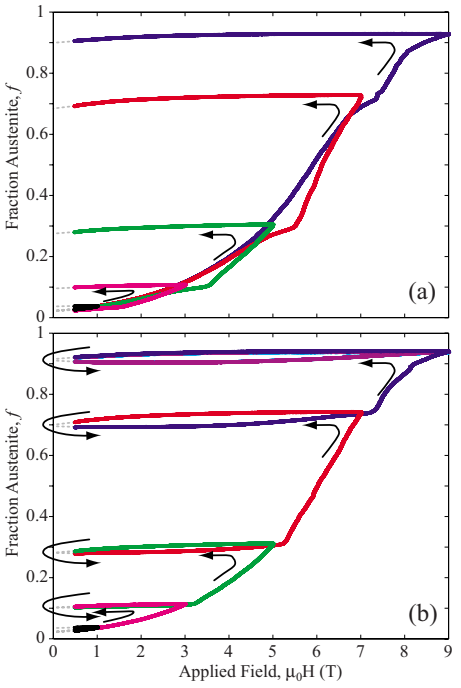

FIG. 7. (Color online) Magnetic field vs mass fraction of austenite, calculated from data in Fig. 7 following (a) method i and (b) method ii. Grey dotted lines indicate likely path of hysteresis curves below 0.5 T. Arrows illustrate direction of magnetic field change over time.

cooled to 150 K to transform it entirely to martensite and was then heated to 190 K. Magnetization was measured while the field was increased to a local maximum (1, 3, 5, 7, or 9 T, sequentially) and then decreased to zero field. Between subsequent demagnetization and remagnetization, sample temperature was decreased to 150 K to revert the sample to martensite [Fig. 6(a)]. (ii) The sample was treated identically to the first approach, except that temperature was held at 190 K throughout the experiment, and was not cooled down in between measurements [Fig. 6(b)]. In method ii, the measurement from 0 to 9 T was repeated three times to determine reproducibility.

Magnetization data were transformed to fraction of austenite present, $f(T)$, following a similar approach as used with thermal hysteresis data. A magnetic hysteresis curve was approximated for pure martensite and pure austenite phases by estimating the extrapolated magnetization of the phases at 190 K from FC and FW curves at a number of magnetic fields (Fig. 6). The representative martensite and cubic Heusler magnetic hysteresis curves shown in Fig. 5 were then scaled to pass through the 190 K data points. The fraction of austenite present was calculated assuming that the total magnetization is proportional to the mass fraction of austenite and martensite phases (Fig. 7). Due to the rapid change in magnetization at low applied fields, as well as the convergence of the martensite and austenite magnetizations, our method led to numerical instabilities below ~0.5 T. This hurdle was encountered because the metric being measured (magnetization) is highly dependent on the stimulus being investigated (magnetic field). Data below ~0.5 T have not been included on Fig. 7. Despite this problem, magnetization is generally an excellent method of calculating $f(T)$ due to the precision of the magnetization measurements.

Application of a magnetic field readily converts martensite to the austenite phase at 190 K, but the removal of the magnetic field leads to only a small degree of recovery (Fig. 7). Cooling the sample down between magnetization measurements to revert to its original state (method i) caused each measurement to follow the same initial magnetization path, while transforming sequentially larger fractions of the sample to the austenite phase. However, sequential runs do have a memory of their previous transformation, as evidenced by kinks in the curve at the previous maximum applied magnetic field (e.g., at ~5 T in the 7 T run). This suggests that either the sample was not entirely reverted to martensite between sequential runs or that defects may have accumulated at the martensite-austenite interfaces, pinning phase boundaries at the previous maximum extent of phase transformation. If temperature is held constant (method ii), a small fraction of austenite, δ, reverts to martensite upon removal of the applied field. As field is reapplied to the previous local maximum, the fraction δ is retransformed to the austenite phase. Application of field beyond the previous local maximum transforms significantly more of the sample to the austenite phase. Decreasing the applied field from a local maximum, H', to zero field and increasing it again to H' define a cyclic transformation that is highly reproducible, as evidenced by the repeated application and removal of a 9 T field.

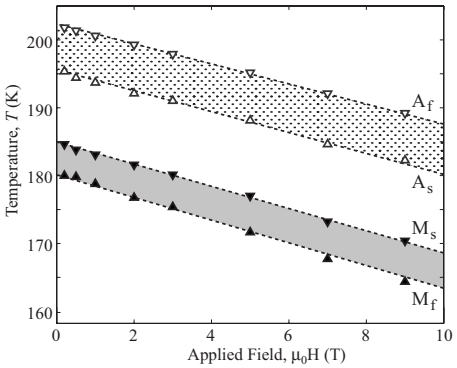

FIG. 8. Dependence of transformation temperatures on applied magnetic field. Best fit lines are shown, calculated with ΔS_{tr} = 1.33 J/mole/K. Gray region represents the transformation to martensite, while the dotted region represents the transformation to the austenite phase.

IV. DISCUSSION

A. Effect of magnetic field on thermal hysteresis

Thermal hysteresis in FC and FW measurements behaves qualitatively similarly at applied fields of 0.2–9 T. The characteristic martensitic transformation temperatures [as defined in Fig. 2(b)] are shown as a function of applied field in Fig. 8. Transition temperatures decrease linearly with an increase in applied magnetic field. The slope of this trend is related to the difference in magnetization (ΔM_{tr}) and entropy (ΔS_{tr}) between the martensite and austenite phases through the magnetic Clausius-Clapeyron equation

$$\frac{dT'}{d(\mu_o H)} = -\frac{M_{aust}(T') - M_{mart}(T')}{S_{aust}(T') - S_{mart}(T')} = -\frac{\Delta M_{tr}}{\Delta S_{tr}}. \quad (1)$$

The entropy change of the transition, ΔS_{tr}, was determined by fitting all four transition temperatures in Fig. 8 ($T' = M_s$, M_f, A_s, and A_f) with least-squares linear models and calculating the mean, ΔS_{tr}^{avg} (Table I). These calculations used the average magnetization differences for each of the four transition temperature trends, as magnetization of the austenite phase was observed to vary significantly over the range of the hysteresis (Fig. 2). The average entropy change of the transition for this alloy is $\Delta S_{tr}^{avg} = 1.33 \pm 0.14$ J/mole/K (19.9 ± 2.1 J/kg/K). This is in good agreement with values of $\Delta S_{tr} = 1.66$ and $\Delta S_{tr} = 1.43$ J/mole/K measured on $Ni_{50}Mn_{35}Sn_{15}$ using scanning calorimetry techniques.[21,26] Thermal hysteresis at very low magnetic fields (0.005 T) does not follow the linear trend of transition temperatures established by moderate- to high-field data because the samples are not magnetically saturated (i.e., ΔM_{tr} is strongly dependent on $\mu_o H$). These data were not included when fitting the temperature vs field trend to determine the entropy change of transition.

TABLE I. Calculated thermodynamic values for $Ni_{50.4}Mn_{34}Sn_{15.6}$.

	$T_{\mu_o H=0}$ [a] (K)	dT/dH (K/T)	ΔM_{tr} (A m^2/kg)	ΔS_{tr} (J/mole K)
M_f	180.5	−1.804	33.26	1.231
M_s	184.8	−1.610	32.42	1.345
A_s	195.3	−1.474	30.56	1.384
A_f	202.1	−1.425	29.37	1.376
ΔS_{tr}^{avg} (J/mole K)	1.33 ± 0.14 [b]			
$\Delta G_{elast}^{M\text{-}P}$ (J/mole)	3.69 ± 0.39 [c]			
$E_{irr}^{M\text{-}P}$ (J/mole)	21.3 ± 2.2 [c]			
$\Delta(\mu_o H)_{comp}$ (T)	15.2			

[a]Value at zero field determined by extrapolating linear best-fit trend.
[b]Uncertainty is 2σ variation.
[c]Uncertainty based on uncertainty of ΔS_{tr}^{avg}.

B. Thermodynamics of thermoelastic phase transition

The thermodynamics of phase transitions are of interest in MCE materials because they affect a material's ability to convert magnetic work efficiently into refrigeration work. For a given phase transition, we may ask (1) what energy barriers must be overcome in order for the transition to proceed and (2) how much energy is irreversibly lost in the process of transformation as hysteresis loss. These terms may be compared against the relative cooling power of the material, which is a measure of a MCE material's ability to perform useful work,[27] to determine the performance of the MCE material. This section briefly presents the existing thermodynamic model for thermoelastic martensitic phase transitions, drawn largely from the work of Ortin and Planes,[28] before estimating both energy barriers to the phase transition (in the form of elastic strain energy) and hysteresis loss.

The thermodynamics of thermoelastic martensitic phase transitions have been extensively studied by numerous authors.[28–33] The principle attributes of the transition are:[28,29] (1) It is a first-order phase transition with two distinct coexisting phases. (2) Lattice mismatch and volume difference between the martensite and austenite phases lead to an elastic strain energy, $\Delta G_{elast}^{M\text{-}P}$, which contributes to the total free energy of the system, leading to a finite two-phase stability region. (3) The transformation process is associated with an irreversible energy loss, $E_{irr}^{M\text{-}P}$, which leads to a hysteresis effect at the transition. (4) Martensite plates nucleate and grow in the austenite phase under conditions of local equilibrium. This equilibrium is defined by the balance of chemical, elastic, and irreversible (dissipative) energy terms at the interface between martensite and austenite phases

$$\Delta G_{chem}^{M\text{-}P} - \Delta G_{elast}^{M\text{-}P} + E_{irr}^{M\text{-}P} = 0. \quad (2)$$

The balance of chemical, elastic, and irreversible energies gives the transition its characteristic shape. For illustrative purposes, the transition may be decomposed by ignoring either the elastic or irreversible terms in Eq. (2) in order to demonstrate their effect on the transition (Fig. 9). In general, elastic energy terms lead to a broadening of the transition and a region of two-phase stability, while irreversible terms lead to energy dissipation and hysteresis. Below, we calculate the magnitude of these two terms in $Ni_{50.4}Mn_{34.0}Sn_{15.6}$.

Elastic energy results from lattice deformations in martensite plates that are constrained to match the volume and

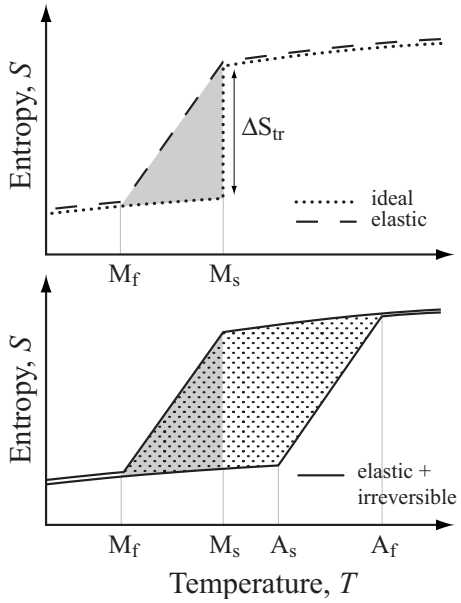

FIG. 9. Characteristic shape of thermoelastic martensitic transition, illustrating elastic and irreversible energy contributions. On an entropy vs temperature diagram, stored elastic energy (ΔG_{elast}) is illustrated by the gray region, while dissipated energy (E_{irr}) is illustrated by the dotted region.

shape of the progenitor austenite crystal grain.[28] Elastic energy limits the extent of reaction that occurs for a given driving force ($\Delta T, \Delta H$), but is fully recoverable during the reverse reaction. Elastic energy may be estimated as[30]

$$\Delta G_{\text{elast}}^{M\text{-}P} = \frac{1}{2}\Delta S_{\text{tr}}\Delta T_{\text{elas}} \tag{3}$$

and is indicated by the gray region in Fig. 9. Here, we define $\Delta T_{\text{elas}}=[(A_f-A_s)+(M_s-M_f)]/2$, averaging the elastic energy calculated from the FC and FW curves. Elastic energy was calculated using zero-field transition temperatures and $\Delta S_{\text{tr}}^{\text{avg}}$ (given in Table I) and is 3.69 ± 0.39 J/mole. Finally, the ratio of the elastic energy to the heat of transition may be estimated as[30]

$$\frac{\Delta G_{\text{elast}}^{M\text{-}P}}{\Delta Q_{\text{tr}}} = \frac{1}{2}\frac{\Delta S_{\text{tr}}\Delta T_{\text{elas}}}{\Delta S_{\text{tr}}M_s} = \frac{1}{2}\frac{\Delta T_{\text{elas}}}{M_s}. \tag{4}$$

In this alloy, elastic energy is ~1.5% of the heat of transition at zero field.

Irreversible energy loss during thermoelastic martensitic transitions arises largely from plastic deformation, friction from interface motion, and creation of defects and is dissipated as heat or acoustic vibrations in the lattice.[28,31,32] Irreversible energy loss is equal to the area within a hysteresis cycle when plotted on entropy and temperature coordinates,[28] as illustrated by the dotted region in Fig. 9(b). Dissipated energy may be estimated as

$$E_{\text{irr}}^{M\text{-}P} = \Delta S_{\text{tr}}\Delta T_{\text{irr}}, \tag{5}$$

where $\Delta T_{\text{irr}}=[(A_f+A_s)-(M_s+M_f)]/2$ is the average thermal hysteresis of the material. This estimate assumes that (1) ΔS_{tr} is constant across the martensitic transition (i.e., that the entropies of the two phases are parallel functions of temperature) and (2) energy is dissipated symmetrically on both the heating and cooling legs of the cycle. Energy dissipated at zero applied field was also estimated from values given in Table I and is 21.3 ± 2.2 J/mole (Table I). As with elastic energy, the ratio between dissipated energy and the heat of transition may be estimated as

$$\frac{E_{\text{irr}}^{M\text{-}P}}{\Delta Q_{\text{tr}}} = \frac{\Delta S_{\text{tr}}\Delta T_{\text{irr}}}{\Delta S_{\text{tr}}M_s} = \frac{\Delta T_{\text{irr}}}{M_s}. \tag{6}$$

In this alloy, irreversible energy loss is ~8% of the heat of transition at zero field.

C. Equivalence of thermal and magnetic hysteresis

Our results demonstrate that both temperature and magnetic field can induce a martensitic phase change in the Ni-Mn-Sn alloy system. These results agree with direct observation of the field-induced martensitic transition by high-field x-ray diffraction experiments.[22] Temperature and field dictate the free energy of martensite and austenite Heusler phases in the Ni-Mn-Sn alloy system through the heat term and Zeeman energy term of the magnetic Gibbs free energy

$$G \equiv U - \mu_o HM - TS, \tag{7a}$$

$$dG = -\mu_o M dH - SdT. \tag{7b}$$

Application of a magnetic field stabilizes the austenite phase relative to the martensite phase due to the higher magnetic moment of the austenite (Fig. 2). Strain and pressure may also induce phase changes through elastic energy[31] and pressure-volume work terms,[33] but these are ignored here.

At the martensite and austenite phase boundary, changes in the thermodynamic variables T and H shift the chemical Gibbs free energy of reaction ($\Delta G_{\text{chem}}^{M\text{-}P}$), inducing a forward or reverse transformation, as described in Eq. (2). An isothermal field change, $\Delta(\mu_o H)$, and an isofield temperature change, ΔT, induce identical extents of reaction if they cause equal changes in the relative free energies of the two phases

$$(dG^M - dG^P)_{\text{isothermal}} = (dG^M - dG^P)_{\text{isofield}} \tag{8}$$

Combining Eqs. (7b) and (8), changes in T and H are related through their coefficients in Eq. (7b)

$$\Delta T\Delta S_{\text{tr}} = \Delta(\mu_o H)\Delta M_{\text{tr}}. \tag{9}$$

In short, an arbitrary change in temperature has an equivalent effect on the phase stability of the system (i.e., on the relative free energies of the two phases) as a magnetic field change given by Eq. (9). Strictly, this assumes that ΔS_{tr} and ΔM_{tr} are independent of temperature and field within the range of temperatures and fields considered.

To test this equivalence, we compared field-induced hysteresis observations (held at 190 K) with temperature-induced hysteresis observations (held at 0.2 T; Fig. 10). Field-induced hysteresis results are those described using method ii in Sec. III B above, while temperature-induced hysteresis observations consisted of successively greater heating and cooling cycles from a base temperature of 190

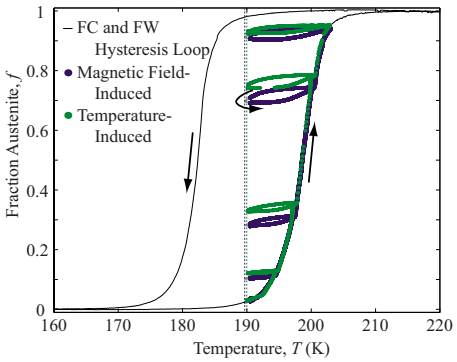

FIG. 10. (Color online) Temperature- ($\mu_0 H=0.2$ T) and field-induced ($T=190$ K) hystereses around the martensite to austenite transition. Field-induced hysteresis data were transformed to the temperature coordinate as described in the text. Interior hysteresis loops in both data sets were timed to start at nearly identical fractions of austenite phase. As in Fig. 8, magnetic hysteresis data below 0.5 T is not included due to difficulty in accurately converting magnetization, M, to fraction transformed, f. Vertical dotted lines represent the base "temperature" of hysteresis loops. Zero-field magnetic hysteresis data corresponds to 189.7 K due to the finite field present in temperature-induced hysteresis data.

K. This temperature was chosen to coincide with the temperature of field-induced hysteresis observations and to guarantee a large phase transformation in response to applied stimuli. The field-induced data were translated to their temperature-induced equivalent by using Eq. (9), with the average difference in magnetization found at A_f ($\Delta M_{\mathrm{tr}}=29.37$ A m^2/kg) and the entropy of transition ($\Delta S_{\mathrm{tr}}=1.33$ J/mole/K), calculated from magnetic data as described previously. The translated field-induced hysteresis behaves identically to the temperature-induced hysteresis; both have the same minimum transformed fraction as the FW curve and both have similar interior hysteresis loops (Fig. 10).

The identical behavior of field- and temperature-induced hystereses suggests that the hysteresis is a fundamental property of the phase transition itself and is therefore independent of the thermodynamic driving force. That is, in both cases, the hysteresis is caused by energy dissipated during the process of nucleation and growth of a new phase, most likely due to internal friction caused by grain-boundary motion.[28,31,32] Therefore, it is the process and extent of phase transformation that dictates the hysteretic behavior, rather than the application of any given environmental stimuli (in this case, temperature or magnetic field).

D. Effect of hysteresis on magnetocaloric effect

Hysteresis reduces the "effective" magnetocaloric effect of a material by both limiting the extent of the phase transition and resulting in dissipative energy loss. In first-order phase change materials, the magnetocaloric effect is due primarily to an applied magnetic field raising or lowering the critical transition temperature (accounting for ΔT_{ad}), and the difference in the entropy between the two phases, ΔS_{tr} (accounting for ΔS_M).[19] If only a fraction of the material transforms from one phase to another, the resulting ΔS_M will decrease proportionally. In the alloy reported here, application and removal of magnetic fields up to 9 T at 190 K resulted in cyclic phase transformations (returning to the identical initial state) of at most 5% of the alloy (Fig. 7, Table II). Therefore, the effective magnetic entropy change at this temperature is at most ~5% of the entropy of transition or $(\Delta S_M)_{\mathrm{eff}} \approx 0.066$ J/mole/K. While the exact extent of phase transformation may differ at other temperatures, it is unlikely to be significantly larger due to the similarity of interior hysteresis loops throughout the transformation (Fig. 4). A larger magnetocaloric effect (more complete phase transformation) may be observed in a single unidirectional experiment, given the proper thermal and magnetic histories of a sample (e.g., the top of Fig. 7). This effect is observed in recent calorimetric experiments which found significantly different ΔS_M depending on the thermal and magnetic-field histories of the sample.[34] However, only transformations measured over a complete cycle of magnetization, demagnetization, and remagnetization will properly account for hysteresis effects inherent in a cyclic refrigeration cycle.

TABLE II. Percent of sample converted cyclically upon application and removal of a magnetic field at 190 K (from Fig. 7).

Applied Field, $\mu_0 H$ (T)	Percent transformed
1	0.2
3	1.2
5	3.4
7	5.0
9	3.5

Complete cyclic phase transformations (100% martensite to 100% austenite phase to 100% martensite) can be induced isothermally by application and subsequent removal of large magnetic fields. The minimum applied field required to induce the complete cyclic transformation is equivalent to a temperature change spanning the entire width of the hysteresis, $\Delta T_{\mathrm{comp}}=(A_f)_{H=0}-(M_f)_{H=0}$, as described in Eq. (9): $\Delta(\mu_o H)_{\mathrm{comp}}=\Delta T_{\mathrm{comp}}\Delta S_{\mathrm{tr}}(A_f)/\Delta M_{\mathrm{tr}}(A_f)\approx 15.2$ T (Table I). This field is significantly higher than the fields attained during our experiments, explaining why we were unable to induce even a complete forward reaction. The present alloy differs significantly from the Ni-Mn-In family of alloys, which have larger ΔM_{tr} and smaller ΔS_{tr}, leading to much lower values of $\Delta(\mu_o H)_{\mathrm{comp}}$ (e.g., ~5.5 T for $Ni_{50.3}Mn_{33.8}In_{15.9}$ based on data presented by Krenke *et al.*[35]). It is important to note that (1) complete cyclic transformations are not possible for $T>(M_f)_{H=0}$, as the sample will never revert to 100% martensite, and (2) for $T<(M_f)_{H=0}$ even larger fields are required to stabilize the austenite phase relative to the martensite phase. We advocate the use of $\Delta(\mu_o H)_{\mathrm{comp}}$ as a metric indicative of the magnitude of applied field necessary to induce complete forward and reverse phase transitions.

In addition to limiting phase transformation, hysteresis loss dissipates useful work that could otherwise transfer heat during a magnetic refrigeration cycle. Hysteresis loss for the

TABLE III. Relative cooling power (RCP=$\Delta S_M \times \delta T_{\mathrm{FWHM}}$) (Ref. 27) of Ni-Mn Heusler alloys.

Composition	RCP (J/mole)	RCP (J/kg)	$\Delta\mu_0 H$ (T)	Source
$Ni_{50}Mn_{37}Sn_{13}$	6.22	95.5	5	Ref. 18
$Ni_{50}Mn_{37}Sn_{13}$	2.22	34.2	2	Ref. 18
$Ni_{50}Mn_{35}Sn_{15}$	6.85	103	5	Ref. 18
$Ni_{50}Mn_{35}Sn_{15}$	2.72	41.0	2	Ref. 18
$Ni_{47}Co_{3.1}Mn_{36.6}Sn_{13.3}$	12.8	196	5	Ref. 39
$Ni_{46.9}Fe_3Mn_{36.8}Sn_{13.3}$	14.0	215	5	Ref. 39
$Ni_{50}Mn_{37}Sb_{13}$	2.78	42.5	5	Ref. 40
$Ni_{50}Mn_{38}Sb_{12}$	3.22	49.7	5	Ref. 40
$Ni_{55.2}Mn_{18.6}Ga_{26.2}$	6.21	102	5	Ref. 41
$Ni_{50}Mn_{34}In_{16}$	12.6	190	5	Ref. 42
$Ni_{50}Mn_{34}In_{14}Ga_2$	9.35	143	5	Ref. 42

complete transformation was estimated as $E_{\mathrm{irr}}^{M\text{-}P} \approx 21.3$ J/mole (319 J/kg) in Sec. IV B using Eq. (5). This is comparable to hysteresis loss measured for martensitic transitions in Cu-27.7%–Al-2.3%–Ni (48–51 J/mole),[36] Cu-7.2%–Zn-23.1%–Al (29 J/mole),[28] and Ti-50.2%–Ni (48 J/mole).[37] For comparison, Table III presents relative cooling powers (RCPs) calculated from data on Ni-Mn Heusler alloys in the literature; the RCP is an estimate of the maximum thermodynamically reversible work that can be performed by the material in a refrigeration cycle, and in first-order phase-transition materials implies complete transformation. The hysteresis loss presented here is about twice the average relative cooling power of typical Ni-Mn Heusler alloys for $\Delta\mu_0 H \sim 5$ T and over three times the relative cooling power of Ni-Mn-Sn alloys with similar compositions.[18] In contrast, a recent study on $Ni_{50}Mn_{34}In_{16}$ found a maximum hysteresis loss of only 7.2 J/mole, as measured by isothermal magnetic hysteresis curves; hysteresis losses in this material for $\Delta\mu_0 H = 4-8$ T were only ~33–45% of the refrigerant capacity (a similar measure to RCP).[20] However, in both cases, hysteresis losses were on the order of the cooling capacity of the material and therefore will significantly reduce the effective cooling capacity of these alloys. Larger fields may induce complete transformation, greatly increasing the cooling capacity of the materials, relative to the hysteresis loss. However, in this particular material, such a field is too large to be practically applicable (~15.2 T).

Hysteresis loss also occurs during partial phase transitions. In these cases, the useful work lost to hysteresis is proportional to the relative area of the hysteresis loop and can be determined by integration of the FC and FW curves of Fig. 4.[38] Hysteresis loss is nearly proportional to the fraction of phase transformed, but the exact relationship is material dependent (Fig. 11). In this alloy, relative hysteresis loss calculated for partial forward and reverse reactions is similar, but not identical, due to the asymmetry of the hysteresis. The relative importance of hysteresis loss and limited phase transformation is uncertain and requires further study in the Heusler alloy system. However, it is clear that hysteresis plays a significant role in limiting a material's utility as a magnetic refrigerant.

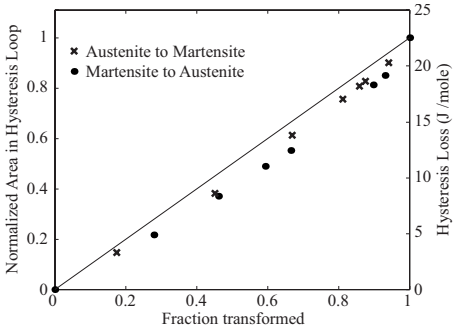

FIG. 11. Hysteresis loss (E_{irr}) for partial temperature-induced phase transitions, calculated assuming E_{irr} is proportional to the area on an f vs T diagram. Linear relationship included as a guide to the eyes.

V. CONCLUSIONS

This paper discusses the hysteresis of the temperature- and magnetic field–induced martensitic phase transition in the Heusler alloy $Ni_{50.4}Mn_{34}Sn_{15.6}$. While Ni-Mn-Sn alloys and other ferromagnetic materials with first-order phase transitions have promising intrinsic magnetocaloric properties, hysteresis effects commonly limit these materials from practical use. However, the exact nature of the interactions between hysteresis and the MCE in these materials has not been thoroughly investigated. Our study draws a number of important conclusions regarding this interaction.

(1) Both temperature and applied magnetic field are thermodynamically equivalent driving forces, inducing complimentary phase transformations and hystereses. Temperature and field are related through the magnetic Gibbs free energy of the transition [Eq. (9)]. This relationship may be used to collapse a complex temperature and magnetic field path onto a single variable for the purpose of constructing a predictive description (e.g., a Preisach model) of the hysteresis.

(2) Elastic and irreversible energy terms limit the extent of the phase transformation induced by a magnetic field. In $Ni_{50.4}Mn_{34}Sn_{15.6}$, the observed hysteresis causes only ~5% of the alloy to cyclicly transform between the martensite and the austenite phase under application and removal of up to a 9 T magnetic field at 190 K. Therefore, only ~5% of the entropy of the transition, ΔS_{tr}, contributes to the magnetocaloric effect (ΔS_M) of the material at this temperature. The field necessary to induce a complete forward and reverse transition is an important material property and may be estimated from Eq. (9). For $Ni_{50.4}Mn_{34}Sn_{15.6}$, $\Delta(\mu_o H)_{\mathrm{comp}} \approx 15.2$ T.

(3) Energy is dissipated at the martensitic transition, detracting from the thermodynamically reversible MCE. Irreversible energy loss directly impacts the efficiency of a magnetic refrigerant. Since higher efficiency is one of the key advantages of magnetic refrigeration, the effect of hysteresis loss on the useful work that can be generated by a material must be considered. In $Ni_{50.4}Mn_{34}Sn_{15.6}$, $E_{\mathrm{irr}}^{M\text{-}P}$ is up to 21.3

J/mole, depending on the fraction of transformation that has taken place. This compares to cooling capacities of ~6.2–6.8 J/mole determined in similar composition NiMnSn alloys.[18] Together, these conclusions suggest that hysteresis effects are as important as thermodynamically reversible entropy and temperature changes when determining the functionality of a magnetocaloric-effect material.

(4) We consider the magnitude of the hysteresis in Heusler alloys to be the primary challenge these materials face as potential magnetic refrigerants. As such, determining pathways to reduce hysteresis is paramount. Future studies in this area may consider thermal processing and alloy composition as both factors are known to influence the magnitude of the hysteresis. Furthermore, the kinetics of the phase transformation process warrants further study as either structural or magnetic relaxation processes may affect hysteresis widths.

ACKNOWLEDGMENTS

We acknowledge A. Pakhomov, J. Cahn, and an anonymous reviewer for critical reviews of this manuscript. We would also like to thank the M. J. Murdock Charitable Trust and Micron Foundation for their support of the Physical Properties Measurement System and XRD Facilities utilized in this study (Department of Materials Science and Engineering, University of Washington). P.J.S. acknowledges support from the DoD and NSF IGERT program.

[1] A. M. Tishin and Y. I. Spichkin, *The Magnetocaloric Effect and its Applications* (IOP, Bristol, 2003), Chap. 1.
[2] V. K. Pecharsky and K. A. Gschneidner, Jr., J. Magn. Magn. Mater. **200**, 44 (1999).
[3] G. V. Brown, J. Appl. Phys. **47**, 3673 (1976).
[4] C. Zimm, A. Jastrab, A. Sternberg, V. Pecharsky, K. J. Gschneidner, M. Osborne, and I. Anderson, Adv. Cryog. Eng. **43**, 1759 (1998).
[5] M. E. Wood and W. H. Potter, Cryogenics **25**, 667 (1985).
[6] A. Giguère, M. Foldeaki, B. Ravi Gopal, R. Chahine, T. K. Bose, A. Frydman, and J. A. Barclay, Phys. Rev. Lett. **83**, 2262 (1999).
[7] K. A. Gschneidner, Jr., V. K. Pecharsky, E. Brück, H. G. M. Duijn, and E. M. Levin, Phys. Rev. Lett. **85**, 4190 (2000).
[8] M. P. Annaorazov, K. A. Asatryan, G. Myalikgulyev, S. A. Nikitin, A. M. Tishin, and A. L. Tyurin, Cryogenics **32**, 867 (1992).
[9] M. P. Annaorazov, M. Unal, S. A. Nikitin, A. L. Tyurin, and K. A. Asatryan, J. Magn. Magn. Mater. **251**, 61 (2002).
[10] V. Provenzano, A. J. Shapiro, and R. D. Shull, Nature (London) **429**, 853 (2004).
[11] R. D. Shull, V. Provenzano, A. J. Shapiro, A. Fu, M. W. Lufaso, J. Karapetrova, G. Kletetschka, and V. Mikula, J. Appl. Phys. **99**, 08K908 (2006).
[12] V. K. Pecharsky and K. A. Gschneidner, Jr., Phys. Rev. Lett. **78**, 4494 (1997).
[13] V. K. Pecharsky and K. A. Gschneidner, Jr., Appl. Phys. Lett. **70**, 3299 (1997).
[14] O. Tegus, E. Brück, K. H. J. Buschow, and F. R. De Boer, Nature (London) **415**, 150 (2002).
[15] H. Wada and Y. Tanabe, Appl. Phys. Lett. **79**, 3302 (2001).
[16] F. X. Hu, X. L. Qian, J. R. Sun, G. J. Wang, X. X. Zhang, Z. H. Cheng, and B. G. Shen, J. Appl. Phys. **92**, 3620 (2002).
[17] A. B. Pakhomov, C. Y. Wong, X. X. Zhang, G. H. Wen, and G. H. Wu, IEEE Trans. Magn. **37**, 2718 (2001).
[18] T. Krenke, E. Duman, M. Acet, E. Wassermann, X. Moya, L. Mañosa, and A. Planes, Nature Mater. **4**, 450 (2005).
[19] V. K. Pecharsky, K. A. Gschneidner, Jr., A. O. Pecharsky, and A. M. Tishin, Phys. Rev. B **64**, 144406 (2001).
[20] V. K. Sharma, M. K. Chatoopadhyay, and S. B. Roy, J. Phys. D **40**, 1869 (2007).
[21] T. Krenke, M. Acet, E. F. Wassermann, X. Moya, L. Mañosa, and A. Planes, Phys. Rev. B **72**, 014412 (2005).
[22] K. Koyama, T. Kanomata, R. Kainuma, K. Oikawa, K. Ishida, and K. Watanabe, Physica B **383**, 24 (2006).
[23] T. LaGrange, G. H. Campbell, P. E. A. Turchi, and W. E. King, Acta Mater. **55**, 5211 (2007).
[24] W. H. Wang, J. L. Chen, Z. H. Liu, G. H. Wu, and W. S. Zhan, Phys. Rev. B **65**, 012416 (2001).
[25] A. C. Larson and R. B. Von Dreele, Los Alamos National Laboratory Report No. LAUR 86-748, 2000 (unpublished).
[26] X. Moya, L. Mañosa, A. Planes, T. Krenke, E. Duman, M. Acet, and E. F. Wassermann, J. Magn. Magn. Mater. **316**, e572 (2007).
[27] K. A. Gschneidner, Jr. and V. K. Pecharsky, Annu. Rev. Mater. Sci. **30**, 387 (2000).
[28] J. Ortín and A. Planes, Acta Metall. **36**, 1873 (1988).
[29] G. B. Olson and M. Cohen, Scr. Metall. **9**, 1247 (1975).
[30] M. Ahlers, R. Pascual, and R. Rapacioli, Mater. Sci. Eng. **27**, 49 (1977).
[31] Y. Deng and G. S. Ansell, Acta Metall. Mater. **38**, 69 (1990).
[32] J. X. Zhang, P. C. W. Fung, and W. G. Zeng, Phys. Rev. B **52**, 268 (1995).
[33] V. A. Chernenko and V. A. L'vov, Philos. Mag. A **73**, 999 (1996).
[34] C. P. Sasso, M. Kuepferling, L. Giudici, V. Baso, and M. Pasquale, J. Appl. Phys. **103**, 07B306 (2008).
[35] T. Krenke, E. Duman, M. Acet, E. F. Wassermann, X. Moya, L. Mañosa, A. Planes, E. Suard, and B. Ouladdiaf, Phys. Rev. B **75**, 104414 (2007).
[36] R. J. Salzbrenner and M. Cohen, Acta Metall. **27**, 739 (1979).
[37] Y. Liu and P. G. McCormick, Acta Metall. Mater. **42**, 2401 (1994).
[38] Y. Deng and G. S. Ansell, Acta Metall. Mater. **39**, 1995 (1991).
[39] T. Krenke, E. Duman, M. Acet, X. Moya, L. Mañosa, and A. Planes, J. Appl. Phys. **102**, 033903 (2007).
[40] M. Khan, N. Ali, and S. Stadler, J. Appl. Phys. **101**, 053919 (2007).
[41] X. Zhou, W. Li, H. P. Kunkel, and G. Williams, J. Phys.: Condens. Matter **16**, L39 (2004).
[42] S. Aksoy, T. Krenke, M. Acet, E. Wassermann, X. Moya, L. Mañosa, and A. Planes, Appl. Phys. Lett. **91**, 241916 (2007).